Research Square

Preprints are preliminary reports that have not undergone peer review.
They should not be considered conclusive, used to inform clinical practice,
or referenced by the media as validated information.

TREM2-independent neuroprotection is mediated by monocyte-derived macrophages in a mouse model of Alzheimer's disease

Raz Dvir-Szternfeld
Weizmann Institute
Giulia Castellani
Weizmann Institute
Michal Arad
Weizmann Institute
Liora Cahalon
Weizmann Institute
Sarah-Phoebeluc Colaiuta
Weizmann Institute
Hadas Keren-Shaul
Weizmann Institute
Tommaso Croese
Weizmann Institute https://orcid.org/0000-0002-3805-3429
Tyler Ulland
Washington University School of Medicine
Marco Colonna
Washington University School of Medicine https://orcid.org/0000-0001-5222-4987
Assaf Weiner
Weizmann Institute of Science
Ido Amit
Weizmann Institute of Science
Michal Schwartz (michal.schwartz@weizmann.ac.il)
Weizmann Institute https://orcid.org/0000-0003-4015-7507

Article

Keywords: Alzheimer's disease, TREM2, disease-associated microglia

Posted Date: December 2nd, 2020

DOI: https://doi.org/10.21203/rs.3.rs-113877/v1

License: This work is licensed under a Creative Commons Attribution 4.0 International License.
Read Full License

Version of Record: A version of this preprint was published at Nature Aging on December 20th, 2021. See the published version at https://doi.org/10.1038/s43587-021-00149-w.

Abstract

The contributions of disease-associated microglia (DAM) and infiltrating monocyte-derived macrophages (MDM) to Alzheimer's disease (AD) are still controversial. Here, using *Trem2*$^{-/-}$5xFAD DAM-deficient mice, we addressed this issue by targeting the programmed cell death ligand-1 (PD-L1) immune checkpoint, shown to modify AD via MDM recruitment. Treating *Trem2*$^{-/-}$5xFAD mice resulted in cognitive improvement, rescue of synapses, and reduction of soluble-amyloid beta $(A\beta)_{1-42}$, with no effect on insoluble $A\beta_{1-42}$. In *Trem2*$^{+/+}$5xFAD mice, the treatment enhanced cognitive performance, led to elevation in DAM levels, and reduced insoluble $A\beta_{1-42}$. Single-cell RNA-sequencing revealed that MDM, derived from both *Trem2*$^{-/-}$ and *Trem2*$^{+/+}$ 5xFAD mouse brains, express a unique set of scavenger receptors and anti-inflammatory genes. Eliminating monocytes abrogated the beneficial effect of anti-PD-L1. The results highlight the need for MDM for neuroprotection even when microglia are fully activated, and demonstrate that their activity occurs through a TREM2-independent mechanism, with the potential to overcome *TREM2* polymorphism in patients.

Introduction

Alzheimer's disease (AD) is a devastating neurodegenerative disorder and the most common cause of dementia. The pathological hallmarks of AD include aggregation of amyloid beta (Aβ) and accumulation of hyperphosphorylated tau protein in the form of neurofibrillary tangles, alongside neuronal dystrophy and neuroinflammation, which manifest in cognitive impairment and gradual memory loss (1). Aβ peptides of different lengths are produced by enzymatic cleavage of the extracellular domain of the amyloid precursor protein (2) with $A\beta_{1-40}$ being the most abundant isoform, and $A\beta_{1-42}$ having the highest tendency to aggregate and greatest potential cytotoxicity (3–6). These peptides aggregate into water-soluble, low-molecular-weight oligomers, which are toxic to synapses (7), and protofibrils and fibrils, which precipitate from the aqueous milieu and tend to form plaques (4).

Based on the numerous failures in attempts to develop a disease-modifying therapy by targeting the plaques and tangles (8, 9), the focus of research has been extended over the last few years towards exploring physiological mechanisms that are responsible for brain maintenance and coping with deviation from homeostasis, including those responsible for removal of debris and dead cells, which might be effective but insufficient, or noneffective and even toxic in AD (1, 9–12). In all other tissues of the body, such mechanisms rely on resident and infiltrating myeloid cells (13–15). In the central nervous system (CNS), the main resident myeloid population is comprised of yolk-sac-derived microglia (16), which can attain various activation states in their response to pathological cues (17), one of which is the disease associated microglia (DAM) (18), identified in the 5xFAD mouse model of amyloidosis (19). Microglia shift from homeostasis to DAM state was shown to be dependent on the activation of 'triggering receptor expressed on myeloid cells 2' (TREM2) (18) a mutation in the gene encoding for it is a major risk factor for late-onset AD (20).

While under pathological conditions, a limited number of monocyte-derived macrophages (MDM) infiltrate the CNS (21), they were shown to have an important role in recovery from acute CNS injuries (22–24) and in containment of AD pathology (25–30), when their number in the CNS is elevated. This was shown to be achieved by several strategies (26, 31, 32), including boosting systemic immunity by targeting the programmed cell death ligand 1 (PD-L1) (33). It remains, however, a subject of ongoing debate, what is the role of the different myeloid populations in the course of neurodegenerative diseases (34–38).

To decipher the contribution of DAM and MDM in coping with AD pathology, we treated *Trem2*$^{-/-}$5xFAD mice (39), which are DAM-deficient (18), with an antibody targeting PD-L1 (anti-PD-L1), previously shown to ameliorate AD pathology through a mechanism involving MDM (33, 40). We found that anti-PD-L1 treatment ameliorated AD pathology and improved cognition in both *Trem2*$^{-/-}$5xFAD and *Trem2*$^{+/+}$5xFAD mice. In both strains, the disease modification was associated with a reduction in the soluble form of $A\beta_{1-42}$. In the *Trem2*$^{+/+}$5xFAD, the treatment effect was accompanied by a reduction in insoluble $A\beta_{1-42}$ and by a modest increase in DAM levels. Single-cell transcriptomic analysis of non-microglia myeloid cells, sorted from the brains of both *Trem2*$^{-/-}$5xFAD and *Trem2*$^{+/+}$5xFAD mice, revealed that MDM expressed a unique group of genes encoding for scavenger receptors shown to be effective in removal of the soluble form of misfolded amyloid protein (41), and for anti-inflammatory activity. Eliminating monocytes, the bone marrow (BM)-derived cells from which macrophages differentiate, using anti-CCR2 monoclonal antibody, abrogated the beneficial effect of the treatment on both cognition and soluble $A\beta_{1-42}$. These results highlight the pivotal role of MDM in mediating the TREM2-independent removal of water-soluble Aβ, sufficient to induce neuroprotection and cognitive improvement, and the contribution of a TREM2-dependent process to removal of insoluble Aβ, with a complementary effect on cognition.

Results

Monocyte-derived macrophages do not contribute to the pool of activated microglia

To decipher the relative contributions of DAM and MDM to disease mitigation, we first examined in *Trem2*$^{+/+}$5xFAD mice whether treatment using PD-L1 blockade affects microglia. To this end, we treated littermate pairs of 6-7 month-old *Trem2*$^{+/+}$5xFAD mice with anti-PD-L1 or IgG2b control antibody, and collected whole brain tissues 14 days later. Single leukocytes ($CD45^+$) were sorted by FACS for massively parallel single cell RNA sequencing (MARS-seq) (42, 43) (**Fig. 1a**). We then applied the metacell algorithm (44) on all cells collected, to identify homogeneous and robust groups of cells (“metacells”), and used differential expression of marker genes to annotate the metacells and classify the different cell types and cell states. In order to enable both qualitative and quantitative characterization of microglia in different activation states, we *in-silico* removed all non-microglial metacells, which together comprised less than 10% of the cells analyzed (Methods). Microglia from both conditions comprised 31 metacells that were annotated manually, according to previously described markers (18), as homeostatic microglia, stage-I-DAM, or DAM (**Fig. 1b**). Quantitative analysis revealed a significantly higher level of DAM in the mice

treated with anti-PD-L1 compared to their IgG2b treated control littermates (average 30% increase; **Fig. 1c, p<0.01**). The increased DAM abundance was not associated with a substantial difference in gene expression pattern between the DAM in the control-IgG2b and the anti-PD-L1 treated groups (**Fig. 1d, Supplementary Figure 1a,b)**.

Next, we examined whether MDM could acquire the DAM signature once infiltrate to the CNS, and thus contribute to the pool DAM. To this end, we generated 5xFAD chimeric mice, transplanted with BM from donors ubiquitously expressing GFP (Ub-GFP) (45). We analyzed cells derived from BM-chimeric 5xFAD mice treated with either anti-PD-L1 or IgG2b control antibody. From each mouse, we separately sorted total leukocytes ($CD45^+$) and BM-derived ($CD45^+GFP^+$) cells for MARS-seq (**Fig. 1e).** The identified metacells were annotated according to differentially expressed canonical marker genes (**Fig. 1f**). Among the $CD45^+GFP^+$ sorted cells, no cells with the DAM signature were identified (**Fig. 1g,h)**, supporting the observation that DAM are derived exclusively from brain-resident microglia (18). Taken together, these findings showed a quantitative change with no qualitative shift in the DAM population following anti-PD-L1 treatment, and with no contribution of MDM to this pool of cells.

Cognitive improvement and reduction of soluble amyloid beta 1-42 in Trem2 deficient mice

The above results encouraged us to test whether anti-PD-L1 treatment would modify the disease in *Trem2*$^{-/-}$5xFAD mice, which lack DAM. To this end, we treated 6-9 month old *Trem2*$^{-/-}$5xFAD mice with either anti-PD-L1 or IgG2b control antibody, and tested their behavior 27-30 days after the treatment. As a positive control for the response to anti-PD-L1 antibody, we also treated *Trem2*$^{+/+}$5xFAD mice. Mice were tested in the Radial Arm Water Maze (RAWM) and the Novel Object Recognition (NOR) tasks, which measure spatial learning and working memory, respectively (**Fig. 2a; Supplementary Figure 2a,b**). Both *Trem2*$^{+/+}$ and *Trem2*$^{/-}$ non-AD mice (WT) from the same cohort were used as cognitively intact controls. In line with previous reports (46), no differences were observed between the *Trem2*$^{-/-}$5xFAD and *Trem2*$^{+/+}$5xFAD mice treated with control-IgG2b (**Fig. 2b,c; Supplementary Figure 2c).** A significant improvement in cognitive ability, assessed by RAWM and NOR tests, was observed in both *Trem2*$^{-/-}$5xFAD and *Trem2*$^{+/+}$5xFAD mice following anti-PD-L1 treatment (**Fig. 2b,c; Supplementary Figure 2c).** However, while in the NOR, the effect of treatment was similar in both groups, in the RAWM, the effect in the *Trem2*$^{-/-}$5xFAD group was slightly but significantly lower (**Fig. 2b,c; Supplementary Figure 2c)**.

The improvement in cognition found above, together with the reported need for TREM2 in the clearance of Aβ plaques (39, 46, 47), prompted us to test whether there was an effect on any form of Aβ in the absence of TREM2. Thus, after cognitive testing, hippocampi were excised, and the soluble (Tris-buffered saline, TBS-soluble) and insoluble (Triton-X-100-soluble) Aβ fractions were analyzed by ELISA. In the hippocampi of *Trem2*$^{-/-}$5xFAD mice, a reduction of the soluble-$A\beta_{1-42}$ was observed, with no change in the insoluble-$A\beta_{1-42}$ (**Fig. 2d**), or in Aβ plaque load (**Supplementary Figure 2d**). In the *Trem2*$^{+/+}$5xFAD mice,

anti-PD-L1 led to a similar reduction in the soluble $A\beta_{1-42}$ (**Fig. 2e**), yet it led also to a reduction in the insoluble $A\beta_{1-42}$ fraction (**Fig. 2e**). These results are in line with previous reports attributing a role to TREM2 in plaque clearance but not in the clearance of soluble $A\beta_{1-42}$ (39, 46, 48). Notably, no change in soluble or insoluble $A\beta_{1-40}$ was observed following the treatment (**Supplementary Figure 2e,f**). As the soluble fraction includes $A\beta_{1-42}$ oligomers, which are known to induce synapto-toxicity (4, 7, 49), we further tested whether the observed effect on soluble Aβ in *Trem2*$^{-/-}$5xFAD mice would be sufficient to protect synapses. To this end, we used brain slices from *Trem2*$^{-/-}$5xFAD mice and evaluated the levels of the presynaptic marker, synaptophysin (19) in the hippocampal regions dentate gyrus (DG) and CA3 following anti-PD-L1 treatment. We found that in both the DG and CA3, the levels of synaptophysin-immunoreactivity were higher in the mice treated with anti-PD-L1 compared to IgG2b-treated group (**Fig. 2f**), as was previously demonstrated in the *Trem2*$^{+/+}$5xFAD strain (40)**.** Overall, the above results suggest that modifying brain function in a mouse model of AD can be achieved in the absence of *Trem2*, and is associated with a reduction in soluble Aβ and rescue of synapses.

Monocyte-derived macrophages express a unique transcriptomic signature that is not dependent of *Trem2*

The effects of the treatment on cognition and soluble $A\beta_{1-42,}$ even in the absence of *Trem2*, and thus in the absence of DAM, led us to question whether the improved cognitive performance in both *Trem2*$^{-/-}$5xFAD and *Trem2*$^{+/+}$5xFAD mice could be attributed to MDM. To this end, we first used MARS-seq to obtain a broad overview of the transcriptomic profiles of the active myeloid populations in the brain. We sorted $CD45^{high}CD11b^{high}$ cells from *Trem2*$^{+/+}$5xFAD and *Trem2*$^{-/-}$5xFAD brains, 14 days after treatment with either anti-PD-L1 or IgG2b control antibody (**Fig. 3a**). Metacell analysis of 1181 non-microglial myeloid cells from both *Trem2*$^{+/+}$5xFAD and *Trem2*$^{-/-}$5xFAD brains resulted in 12 metacells. Equal number of microglia from the same pool of mice were sampled as a reference. Metacells were clustered and annotated, according to differentially expressed canonical marker genes, as homeostatic microglia, stage-1-DAM, DAM, three monocytes states, and three MDM cell states (**Fig. 3a**). While DAM, as expected, were absent from the *Trem2*$^{-/-}$5xFAD mice (**Fig. 3b,c**), MDM were present in both *Trem2*$^{+/+}$5xFAD and *Trem2*$^{-/-}$5xFAD brains, sharing similar transcriptomic profiles (**Fig. 3b,c**)**.** Among the three states of MDM observed, MDM-1 were found to uniquely express anti-inflammatory genes (e.g., Mannose receptor C-type 1 (Mrc1)) and a unique repertoire of molecules, including scavenger receptors such as Stabilin 1 (Stab1), CD163, and Macrophage scavenger receptor 1 (Msr1) (**Fig. 3d,e)**, which can contribute to the clearance of neurotoxic misfolded proteins from the brain (41). MDM-3 seemed to be the most recently infiltrating cells, expressing high levels of C-C chemokine receptor type 2 (Ccr2), and MDM-2 could represent an intermediate stage. Analysis of differential gene expression between MDM-1 and DAM, revealed their non-redundant profiles (**Fig. 3e, Supplementary Figure 3**). The majority of functional genes expressed by MDM-1 were not expressed by DAM, except for Apolipoprotein E (Apoe), which was

highly expressed by both (**Fig. 3e)** and is a known AD 'risk factor' gene that is required for the removal of Aβ (50).

Eliminating monocytes abrogated the beneficial effects of immune checkpoint blockade on cognition and on soluble Aβ removal

Since the signature of MDM in *Trem2*$^{-/-}$5xFAD was similar to that found in *Trem2*$^{+/+}$5xFAD, we tested whether they are necessary for modifying AD in the absence of DAM. To this end, we treated *Trem2*$^{-/-}$5xFAD mice, with anti-PD-L1 antibody, along with CCR2-blocking antibody (anti-CCR2) to deplete monocytes, as was previously reported (22, 51). The anti-CCR2 antibody was systemically injected to *Trem2*$^{-/-}$5xFAD mice, starting from 3 days before anti-PD-L1 treatment and continuing every 3 days, until day 9 post-treatment, to ensure the complete elimination of monocytes throughout the entire critical period of their homing to the brain (22, 23). Cognitive performance was assessed by the RAWM and NOR tasks 27-30 days after the anti-PD-L1 treatment, and subsequently, hippocampal tissues were excised for ELISA (**Fig. 4a**). Anti-CCR2 antibody completely abrogated the beneficial effect of anti-PD-L1 on cognitive performance. (**Fig. 4b,c**). No effect on locomotion or on anxiety was found due to anti-PD-L1 or anti-CCR2 treatment (**Supplementary Figure 4d,e**), which further supports the contention that MDM contributed to the improved cognitive performance. The level of soluble $A\beta_{1\text{-}42}$ was lower by approximately 40% in mice treated with anti-PD-L1 alone compared to the group treated with anti-PD-L1 and anti-CCR2 (**Fig. 4e**), suggesting that anti-PD-L1 effect was dampened by CCR2-blockade. As expected, the levels of insoluble $A\beta_{1\text{-}42}$ in the *Trem2*$^{-/-}$5xFAD mice treated with anti-PD-L1 and anti-CCR2 were not different from those treated with anti-PD-L1 alone (**Fig. 4e**). Moreover, a strong correlation was found between RAWM performance and the levels of soluble $A\beta_{1\text{-}42}$ in the *Trem2*$^{-/-}$5xFAD mice (**Fig. 4f**). Of note, in the *Trem2*$^{+/+}$5xFAD mice, depletion of monocytes completely abrogated the beneficial effect of anti-PD-L1 treatment on NOR but only partially on RAWM (**Supplementary Figure 4a-c**), which could suggest an additional TREM2-dependent mechanism, presumably related to the increased level of DAM induced by the treatment in these mice (**Fig. 1c**). Overall, we show here that MDM are key players in cognitive improvement following anti-PDL1 immunotherapy, in both *Trem2*$^{+/+}$5xFAD and *Trem2*$^{-/-}$5xFAD mice.

Discussion

In the present study, we found in mouse models of amyloidosis, that MDM display a *Trem2*-independent neuroprotective role, associated with the removal of soluble $A\beta_{1-42}$, which could be obtained by boosting the immune system via targeting PD-L1. In the presence of *Trem2*, an additional complementary mechanism was activated following the same treatment, associated with elevation of DAM and with the removal of insoluble $A\beta_{1-42}$.

The pivotal role of MDM in AD modification was demonstrated when *Trem2*$^{-/-}$5xFAD mice, depleted of monocytes, were treated with anti-PD-L1 antibody. Thus, in the absence of monocytes, no beneficial effect of the treatment was found on working and spatial memory, nor on the levels of soluble $A\beta_{1-42}$. Of note, the beneficial effect of anti-PD-L1 treatment in the *Trem2*$^{+/+}$5xFAD was slightly but significantly stronger than that observed in *Trem2*$^{-/-}$5xFAD mice, only in the RAWM but not in the NOR. As a corollary, the beneficial effect was completely lost following monocyte depletion in the *Trem2*$^{+/+}$5xFAD in the NOR but only partially lost in the RAWM. The differences between the observed results in the RAWM and NOR in *Trem2*$^{+/+}$5xFAD could reflect differences in the sensitivity of the two assays (52). Alternatively, these differences might be due to the distinct functions assessed by the RAWM and NOR, spatial versus working memory. Accordingly, it is possible that the activity of DAM, the abundance of which was elevated following anti-PD-L1 treatment in *Trem2*$^{+/+}$5xFAD, contributed more to spatial memory than to working memory, via, at least in part, the reduction of insoluble $A\beta_{1-42}$.

Single cell RNA-seq revealed that the increased level of DAM following anti-PD-L1 treatment reflected changes in the proportion of the total microglia, and was not accompanied by any transcriptomic changes in their signature. This argues in favor of enhanced activation of resting microglia in the same TREM2-dependent pathway previously reported (18), rather than proliferation or rescue of exhausted DAM. In addition, it is important to note that our experiments using BM-chimeric *Trem2*$^{+/+}$5xFAD mice, which enabled the distinction between BM-derived cells and resident microglia, ruled out the possibility that the observed elevation in DAM might be an outcome of infiltration of MDM that acquired a DAM signature, in line with previous studies (18, 53, 54).

Characterization of non-microglial myeloid cells by MARS-seq, revealed that a subgroup of MDM, present in both T*rem2*$^{-/-}$ and *Trem2*$^{+/+}$5xFAD mice, express a transcriptomic signature of genes associated with anti-inflammatory and phagocytic activities. Although some of the genes expressed by MDM-1 were previously found to be expressed by macrophages in WT mouse brains (55), the MDM observed here in AD, expressed additional functional genes, such as the scavenger receptor MSR-1, which was shown to be required for clearing the soluble $A\beta_{1-42}$ oligomers (41). Recently, MSR1-expressing macrophages were also shown to be important in resolution of sterile inflammation in the brain, following stroke, through Damage-Associated Molecular Patterns (DAMP) (56). This further indicates that boosting MDM homing to the brain helps contain chronic neurodegenerative diseases regardless of the disease etiology, in line with numerous independent studies in several different brain pathologies (57–62). Following anti-PD-L1 treatment in a tauopathy mouse model, a macrophage signature similar to that of MDM-1, including the expression of MSR-1, was found (40). The potential ability of these cells to remove toxic forms of misfolded proteins, via recognition of molecular patterns, could explain why the same treatment, targeting the PD-1/PD-L1 pathway, is effective in different AD mouse models. We cannot rule out the possibility that MDM also contribute to the clearance of toxic molecules via expression of additional molecules, such as APOE.

While the reduction of insoluble $A\beta_{1-42}$ and of Aβ plaques was found to require TREM2, in line with previous publications (39, 46, 47), treatment with anti-PD-L1 was shown to reduce the soluble fraction of $A\beta_{1-42}$ in a Trem2-independent manner. Thus, the effect of the treatment on Aβ plaques could be simply an outcome of the prevention of its accumulation, and therefore, secondary to the effect on soluble $A\beta_{1-42}$ and less crucial for cognitive improvement. This further explains why using plaque burden as a single readout for the efficacy of PD-1/PD-L1 blockade in AD is not sufficiently informative (63). In a recent study, assessing multiple parameters in APP/PSN1 mice, it was reported that treatment with anti-PD-1 antibody led to improved cognitive performance and reduced disease pathology, measured by biochemical parameters and plaque burden (32).

The ELISA assay used for determining levels of Aβ in the soluble fraction recognizes the 1–42 peptide in all water-soluble conformational forms, ranging from monomers, which are essential for synaptic activity, and up to dodecamers, which are toxic to synapses (3, 4, 64). Notably, the observed reduction by approximately 30% of water soluble $A\beta_{1-42}$ following anti-PD-L1 treatment, might represent the removal of the entire fraction of toxic oligomers, which was sufficient to achieve disease modification and rescue of function. Our results are consistent with the most recent version of the amyloid cascade hypothesis, suggesting that the soluble aggregates of $A\beta_{1-42}$ are a major species responsible for neuronal dysfunction, collectively termed oligomeropathy (65). Our results are also consistent with accumulated evidence from clinical trials highlighting the lack of correlation between amyloid plaque distribution and disease severity, and arguing against a direct pathogenic role of Aβ plaques in AD (66). The stability of Aβ oligomers and their dynamics are still unclear, but their overall formation might be closely related to the early low-grade inflammation seen during disease development (67, 68).

Altogether, our findings support the approach of empowering the immune system to facilitate MDM mobilization as a shared mechanism of repair for treating AD patients, regardless of whether these patients carry mutations in the *TREM2* gene or in a TREM2-related pathway.

Materials And Methods

Mice:

Two mouse models were used in this study: heterozygous 5xFAD transgenic mice (on a C57/BL6-SJL background), which overexpress familial AD mutant forms of human APP (the Swedish mutation, K670N/M671L; the Florida mutation, I716V; and the London mutation, V717I) and PS1 (M146L/L286V) transgenes under the transcriptional control of the neuron-specific mouse Thy-1 promoter (19) (5xFAD line Tg6799; The Jackson Laboratory), and *Trem2*$^{-/-}$5xFAD mice. *Trem2*$^{-/-}$5xFAD and *Trem2*$^{+/+}$5xFAD were obtained from the laboratory of Marco Colonna (Washington University, St. Louis), where they were generated as previously described (69). For bone-marrow transplantation assays, donor cells were isolated from C57BL/6 CD45.2 Ub-GFP mice in which GFP is ubiquitously expressed (45). All mice were bred and maintained at the animal breeding center of the Weizmann Institute of Science. For the period of cognitive assessments, mice were kept on a reversed light-dark cycle. All experiments described complied

with the regulations formulated by the Institutional Animal Care and Use Committee (IACUC) of the Weizmann Institute of Science. In all experiments, mice were anesthetized and transcardially perfused with phosphate buffered saline (PBS) before tissue dissection.

Preparation of BM chimeras:

Chimeras were prepared by subjecting recipient mice to lethal irradiation (950 rad), directing the beam to the lower part of the body, and avoiding the head (22). The following day, bone marrow (BM) cells were isolated from the tibiae and femur leg bones of Ub-GFP mice and filtered through a 70 μm cell strainer. Each recipient mouse was then reconstituted with 5×10^6 BM intravenously injected cells of gender-matched donors. The recipient mice were analyzed 5-8 weeks after BM transplantation to determine the extent of chimerism.

Therapeutic antibodies:

For PD-L1 blockade, PD-L1-blocking antibody directed to mouse PD-L1 (anti-PD-L1 antibody, clone 10F.9G2 BIOX-CELL) or an isotype control (anti-keyhole limpet hemocyanin; clone LTF-2 BIOXCELL), were administered i.p. at an effective dose of 1.5 mg/mouse (40).

Single cell sorting:

After perfusion with PBS, supplemented with 1% L-glutamine, brains were excised without olfactory bulb and brain stem, and manually chopped to pieces (0.5-1 mm2 in size), prior to a software-controlled dissociation by gentle MACS™ in PBS. For density gradient separation, the pellet was resuspended with 40% Percoll, and centrifuged at 750 G for 20 min at 20 °C; the supernatant was then discarded. Cells were suspended in ice-cold sorting buffer (PBS supplemented with 2mM EDTA and 2% FCS) supplemented with anti-mouse CD16/32 (BD Bioscience) to block Fc receptors before labeling with fluorescent antibodies against cell-surface epitopes. Samples were stained using the following antibodies: BV421-conjugated CD45, PE-conjugated CD45, PE-conjugated CD11b. For sorting, samples were gated for CD45+ after exclusion of debris and doublets, and further gated according to the experimental design. Cell populations were sorted using either SORP-aria (BD Biosciences) or ARIA-III instruments (BD Biosciences), and analyzed using BD FACSDIVA (BD Biosciences) software. Isolated single cells were sorted into 384-well cell capture plates containing 2 μL of lysis solution and barcoded poly(T) reverse-transcription (RT) primers for single-cell RNA-seq (42). Four empty wells were kept in each 384-well plate as a no-cell control. Immediately after sorting, each plate was spun down to ensure cell immersion in the lysis solution, snap frozen on dry ice, and stored at –80°C until processing.

Massively Parallel Single-Cell RNA-seq library preparation (MARS-seq2.0):

Single-cell libraries were prepared according to the MARS-seq2.0 protocol (43). In brief, mRNA was isolated from cells sorted into capture plates, barcoded and converted into cDNA, and pooled using an automated pipeline. The pooled sample was then linearly amplified by T7 *in-vitro* transcription, and the resulting RNA was fragmented and converted into a sequencing-ready library by tagging the samples with pool of barcodes and Illumina sequences during ligation, RT, and PCR. Each pool of cells was tested for library quality and concentration, assessed as previously described (43).

Analysis of MARS-seq data:

Single cell RNA-seq libraries (pooled at equimolar concentrations) were sequenced on an Illumina NextSeq 500 at a median sequencing depth of ~20,000 reads per cell. Sequences were mapped to the mouse genome (mm10), demultiplexed and filtered as previously described (42, 43) with the following adaptations: mapping of reads was done using HISAT (v.0.1.6) and reads with multiple mapping positions were excluded. Reads were associated with genes if they were mapped to an exon, using the UCSC Genome Browser for reference. The level of spurious unique molecular identifiers (UMIs) in the data were estimated by using statistics on empty MARS-seq wells, and excluded rare cases with estimated noise > 5%. We used the R package “MetaCell” (44) to generate homogenous and robust groups of cells in each analysis. We removed specific mitochondrial genes, immunoglobulin genes, and genes linked with poorly supported transcriptional models (annotated with the prefix “Rp-”). We then filtered cells with less than 400 UMIs. Feature genes were selected using the parameter Tvm = 0.8 and a minimum total UMI count > 50. In all the analysis of all experiments, microglia were identified according to the expression of Hexb gene.

$A\beta_{1-40}$ and $A\beta_{1-42}$ ELISA:

For these experiments, tissues from 7-10 month-old mice were used. Following intracardial PBS perfusion of the mice, the hippocampi were collected from one or both brain hemispheres, as indicated in the legends, and immediately frozen and stored at -80°C. The samples were homogenized in TBS solution [Tris, pH 7.4 (50 mM), NaCl (150 mM)], EDTA (2mM), and 1% Protease Inhibitor Cocktail (Sigma Aldrich) using the Micro Tube homogenizer with plastic pestles. The lysates were then centrifuged for 40 minutes at 350,000 g in 500 µl Polycarbonate centrifuge tubes (Beckman Coulter) at 4°C in an Optima MAX-XP Ultracentrifuge with a TLA 120.1 rotor (Beckman Coulter). The supernatant was collected and stored at -80°C as “TBS-soluble fraction” ready for further ELISA assay. The pellet was completely resuspended in Triton-X-100 solution [Tris, pH 7.4 (50 mM), NaCl (150 mM), 1% Triton X-100 (Sigma Aldrich), 1% Protease

Inhibitor Cocktail (Sigma Aldrich)]. After 15 min incubation at 4°C, the samples were centrifuged for 40 minutes at 350,000 g at 4°C, and the supernatant was collected as “Triton-X-100-soluble fraction” and stored at -80°C. BCA assay (Pierce BCA Protein Assay Kit) was performed to determine the protein concentrations in both TBS-soluble (also referred as “soluble”) and Triton-X-100-soluble (or “insoluble”) fractions. In the experiments presented in Figure 2, LEGEND MAX β-Amyloid x-40 and x-42 ELISA Kits (BioLegend) were used to measure $A\beta_{1\text{-}40}$ and $A\beta_{1\text{-}42}$ peptide levels, respectively, following the manufacturer’s instructions, in the experiments presented in Figure 4, human $A\beta_{42}$ Ultrasensitive ELISA Kit (Invitrogen) was used to measure $A\beta_{1\text{-}42}$ levels, according to the manufacturer’s instructions.

Blocking CCR2:

For depletion of CCR2-expressing cells, anti-CCR2 monoclonal antibody, MC21was injected i.p. (400µg) every 4 days. No effect on behavior was observed in wild type animals.

Immunohistochemistry:

After perfusion with PBS, brain tissues were excised and fixated. Paraffin-embedded sections were prepared, as previously described (31). The following primary antibodies were used: mouse anti-Aβ (1:300, Covance, #SIG-39320) and rabbit anti-synaptophysin (1:100, Abcam, #32127). Secondary antibodies included: Cy2-conjugated donkey anti-mouse and Cy3-conjugated donkey anti-rabbit antibodies (1:200; all from Jackson Immunoresearch) Microscopic analysis was performed using a fluorescence microscope (E800; Nikon) equipped with a digital camera (DXM 1200F; Nikon), and with a ×20 NA 0.50 objective lens (Plan Fluor; Nikon). Representative images were taken using confocal microscopy (Zeiss, LSM880), with 20x objective lens.

Aβ plaque quantitation:

From each brain, 6 µm sagittal slices were made, and four sections per mouse were immunostained. Histogram-based segmentation of positively stained pixels was performed using Image-Pro Plus software (Media Cybernetics, Bethesda, MD, USA). The segmentation algorithm was manually applied to each image, in the DG area, and the percentage of the area occupied by total Aβ immunostaining, selected for minimal size, was determined. Plaque numbers were quantified from the same 6 µm sagittal brain slices, and are presented as the average number of plaques per brain region, in the region of interest (ROI), identically marked on all slides from all animals examined. Prior to quantification, slices were coded to mask the identity of the experimental groups, and were quantified by an observer blinded to the identity of the groups.

Radial Arm Water Maze (RAWM):

RAWM was used to test hippocampal-dependent spatial learning, following the protocol of Alamed and colleagues (70) with some modifications. Briefly, six stainless-steel inserts were placed in a plastic pool, forming six open and connected arms. A hidden platform was placed at the end of a 'goal arm' (**arm 6; Supplementary Figure 2a**). Milk powder was used to make the water opaque, and the water was maintained at a temperature of 23±1°C. On day 1, training phase, mice were subjected to 15 trials. In each trial, a mouse was given 60 sec to find the platform. A mouse that failed in finding the platform, was placed on it by the experimenter. Inter-trial interval (ITI) was, on average, 20 min. Trials alternated between a visible and hidden platform. However, from trial 12 and throughout the second day, the platform was hidden. Spatial learning and memory were measured by an investigator who was blinded to the treatment of the mice, and who recorded the number of arm entry errors (error was defined as entrance to an incorrect arm, or a failure to enter any arm within 15 sec) as well as the escape latency of the mice on each trial. The 30 trials were grouped into 3-trial bins – 5 bins on day 1, and 5 bins on day 2. Data were analyzed by a team member who did not perform the experiment.

Novel Object Recognition (NOR) task

The NOR protocol was modified from Bevins and Besheer (71), and used a 41.5 x 41.5 cm gray apparatus. The experiment spanned 2 days and included three trials: a habituation trial – a 20 min session in the empty apparatus (day 1), familiarization trial – a 10 min session presenting two identical objects located 15 cm apart (day 2); and a test trial – following a 1 hour training-to-testing interval, each mouse was returned to the apparatus for a 6 min session in which one of the objects was replaced by a novel one (see **supplementary, Figure 2b**). Mouse behavior was recorded and analyzed by an investigator who was blinded to the treatment group. Novel object preference was defined as "discrimination ratio" = time (sec) spent with novel object / (time spent with familiar object + time spent with novel object). Locomotor activity was measured as distance moved (cm/day) in the empty arena during the day of the habituation. The time spent in the center of the arena was recorded to assess anxiety.

Statistical analysis

A paired student's t-test (one-tail) was performed to assess the difference in percentage of DAM out of total microglia cells **(Fig. 1c).** Unpaired student's t-tests (one tail) were used to analyze the data of immunostaining measurements **(Fig. 2f, Supplementary Figure 2d)** and ELISA with two groups (**Fig. 4e**). One-way ANOVAs were used to analyze the data of ELISA **(Fig. 2d,e, Supplementary Figure 2e,f)**, and NOR **(Fig. 2c, Fig. 4d and Supplementary Figure 4c)**, as well as of activity (**Supplementary Fig. 4d**) and anxiety (**Supplementary Figure 4e**) measurements collected at NOR test habituation phase. Two-way ANOVAs

with repeated measures (one for latency and one for errors were used to analyze RAWM data (**Fig. 2b, Fig. 4b,c and Supplementary Fig. 2c**). ANOVAs identifying a significant result were followed by a Fisher's LSD test for multiple comparisons. Pearson correlation was used to determine the correlation between RAWM performance (time to platform) and the levels of soluble $A\beta_{1-42}$ (**Fig. 4f**). Differential gene expression analysis (**Fig. 3e, Supplementary Fig. 3)** was performed upon down-sampling of the UMI matrix as part of the MetaCell package on molecules/1,000 UMIs by Mann-Whitney U test with false-discovery rate (FDR) correction.

Declarations

Data and Software Availability. Raw and processed sequencing data will be available at the time of publication. The codes will be available upon acceptance of the manuscript.

ACKNOWLEDGEMENTS We thank Dr. Shelley Schwarzbaum for editing the manuscript. Research in the M.S. lab is supported by Advanced European Research Council grants (741744); Israel Science Foundation (ISF)-research grant no. 991/16; and ISF-Legacy Heritage Bio-Medical Science Partnership-research grant no. 1354/15. We wish to thank the Adelis and Thompson Foundations for their generous support of our AD research. I.A. is an incumbent of the Eden and Steven Romick Professorial Chair, supported by Merck KGaA, Darmstadt, Germany, the Chan Zuckerberg Initiative (CZI), the HHMI International Scholar award, the European Research Council Consolidator Grant (ERC-COG) 724471-HemTree2.0, an SCA award of the Wolfson Foundation and Family Charitable Trust, the Thompson Family Foundation, an MRA Established Investigator Award (509044), the Israel Science Foundation (703/15), the Ernest and Bonnie Beutler Research Program for Excellence in Genomic Medicine, the Helen and Martin Kimmel award for innovative investigation, the NeuroMac DFG/Transregional Collaborative Research Center Grant, an International Progressive MS Alliance Grant/NMSS PA-1604 08459, and an Adelis Foundation Grant.

Author contributions

R.D.S., G.C., M.A. and A.W. contributed to the design and performance of the experiments, under the guidance of M.S. and I.A. All these authors contributed to the writing of the manuscript.

Competing interests

M.S. is an inventor of the intellectual property that forms the basis for development of PD-L1 immunotherapy for AD.

References

1. Masters CL, Bateman R, Blennow K, Rowe CC, Sperling RA, Cummings JL. 2015. Alzheimer's disease. *Nat Rev Dis Primers* 1: 15056
2. Masters CL, Selkoe DJ. 2012. Biochemistry of amyloid beta-protein and amyloid deposits in Alzheimer disease. *Cold Spring Harb Perspect Med* 2: a006262
3. Lesne S, Koh MT, Kotilinek L, Kayed R, Glabe CG, Yang A, Gallagher M, Ashe KH. 2006. A specific amyloid-beta protein assembly in the brain impairs memory. *Nature* 440: 352-7
4. Bernstein SL, Dupuis NF, Lazo ND, Wyttenbach T, Condron MM, Bitan G, Teplow DB, Shea JE, Ruotolo BT, Robinson CV, Bowers MT. 2009. Amyloid-beta protein oligomerization and the importance of tetramers and dodecamers in the aetiology of Alzheimer's disease. *Nat Chem* 1: 326-31
5. Shea D, Hsu CC, Bi TM, Paranjapye N, Childers MC, Cochran J, Tomberlin CP, Wang L, Paris D, Zonderman J, Varani G, Link CD, Mullan M, Daggett V. 2019. alpha-Sheet secondary structure in amyloid beta-peptide drives aggregation and toxicity in Alzheimer's disease. *Proc Natl Acad Sci U S A* 116: 8895-900
6. Sengupta U, Nilson AN, Kayed R. 2016. The Role of Amyloid-beta Oligomers in Toxicity, Propagation, and Immunotherapy. *EBioMedicine* 6: 42-9
7. Ferreira ST, Lourenco MV, Oliveira MM, De Felice FG. 2015. Soluble amyloid-beta oligomers as synaptotoxins leading to cognitive impairment in Alzheimer's disease. *Front Cell Neurosci* 9: 191
8. Panza F, Lozupone M, Logroscino G, Imbimbo BP. 2019. A critical appraisal of amyloid-beta-targeting therapies for Alzheimer disease. *Nat Rev Neurol* 15: 73-88
9. Giacobini E, Gold G. 2013. Alzheimer disease therapy--moving from amyloid-beta to tau. *Nat Rev Neurol* 9: 677-86
10. Congdon EE, Sigurdsson EM. 2018. Tau-targeting therapies for Alzheimer disease. *Nat Rev Neurol* 14: 399-415
11. Dong Y, Li X, Cheng J, Hou L. 2019. Drug Development for Alzheimer's Disease: Microglia Induced Neuroinflammation as a Target? *Int J Mol Sci* 20
12. Tam C, Wong JH, Ng TB, Tsui SKW, Zuo T. 2019. Drugs for Targeted Therapies of Alzheimer's Disease. *Curr Med Chem* 26: 335-59
13. Wynn TA, Vannella KM. 2016. Macrophages in Tissue Repair, Regeneration, and Fibrosis. *Immunity* 44: 450-62
14. Minutti CM, Knipper JA, Allen JE, Zaiss DM. 2017. Tissue-specific contribution of macrophages to wound healing. *Semin Cell Dev Biol* 61: 3-11
15. Peiser L, Mukhopadhyay S, Gordon S. 2002. Scavenger receptors in innate immunity. *Curr Opin Immunol* 14: 123-8
16. Ginhoux F, Prinz M. 2015. Origin of microglia: current concepts and past controversies. *Cold Spring Harb Perspect Biol* 7: a020537

17. Hanisch UK, Kettenmann H. 2007. Microglia: active sensor and versatile effector cells in the normal and pathologic brain. *Nat Neurosci* 10: 1387-94
18. Keren-Shaul H, Spinrad A, Weiner A, Matcovitch-Natan O, Dvir-Szternfeld R, Ulland TK, David E, Baruch K, Lara-Astaiso D, Toth B, Itzkovitz S, Colonna M, Schwartz M, Amit I. 2017. A Unique Microglia Type Associated with Restricting Development of Alzheimer's Disease. *Cell* 169: 1276-90 e17
19. Oakley H, Cole SL, Logan S, Maus E, Shao P, Craft J, Guillozet-Bongaarts A, Ohno M, Disterhoft J, Van Eldik L, Berry R, Vassar R. 2006. Intraneuronal beta-amyloid aggregates, neurodegeneration, and neuron loss in transgenic mice with five familial Alzheimer's disease mutations: potential factors in amyloid plaque formation. *J Neurosci* 26: 10129-40
20. Guerreiro R, Wojtas A, Bras J, Carrasquillo M, Rogaeva E, Majounie E, Cruchaga C, Sassi C, Kauwe JS, Younkin S, Hazrati L, Collinge J, Pocock J, Lashley T, Williams J, Lambert JC, Amouyel P, Goate A, Rademakers R, Morgan K, Powell J, St George-Hyslop P, Singleton A, Hardy J, Alzheimer Genetic Analysis G. 2013. TREM2 variants in Alzheimer's disease. *N Engl J Med* 368: 117-27
21. Ajami B, Bennett JL, Krieger C, Tetzlaff W, Rossi FM. 2007. Local self-renewal can sustain CNS microglia maintenance and function throughout adult life. *Nat Neurosci* 10: 1538-43
22. Shechter R, London A, Varol C, Raposo C, Cusimano M, Yovel G, Rolls A, Mack M, Pluchino S, Martino G, Jung S, Schwartz M. 2009. Infiltrating blood-derived macrophages are vital cells playing an anti-inflammatory role in recovery from spinal cord injury in mice. *PLoS Med* 6: e1000113
23. Shechter R, Miller O, Yovel G, Rosenzweig N, London A, Ruckh J, Kim KW, Klein E, Kalchenko V, Bendel P, Lira SA, Jung S, Schwartz M. 2013. Recruitment of beneficial M2 macrophages to injured spinal cord is orchestrated by remote brain choroid plexus. *Immunity* 38: 555-69
24. Gadani SP, Walsh JT, Smirnov I, Zheng J, Kipnis J. 2015. The glia-derived alarmin IL-33 orchestrates the immune response and promotes recovery following CNS injury. *Neuron* 85: 703-9
25. Butovsky O, Koronyo-Hamaoui M, Kunis G, Ophir E, Landa G, Cohen H, Schwartz M. 2006. Glatiramer acetate fights against Alzheimer's disease by inducing dendritic-like microglia expressing insulin-like growth factor 1. *Proc Natl Acad Sci U S A* 103: 11784-9
26. Koronyo Y, Salumbides BC, Sheyn J, Pelissier L, Li S, Ljubimov V, Moyseyev M, Daley D, Fuchs DT, Pham M, Black KL, Rentsendorj A, Koronyo-Hamaoui M. 2015. Therapeutic effects of glatiramer acetate and grafted CD115+ monocytes in a mouse model of Alzheimer's disease. *Brain* 138: 2399–422
27. Koronyo-Hamaoui M, Ko MK, Koronyo Y, Azoulay D, Seksenyan A, Kunis G, Pham M, Bakhsheshian J, Rogeri P, Black KL, Farkas DL, Schwartz M. 2009. Attenuation of AD-like neuropathology by harnessing peripheral immune cells: local elevation of IL-10 and MMP-9. *J Neurochem* 111: 1409-24
28. Simard AR, Soulet D, Gowing G, Julien JP, Rivest S. 2006. Bone marrow-derived microglia play a critical role in restricting senile plaque formation in Alzheimer's disease. *Neuron* 49: 489-502
29. Town T, Laouar Y, Pittenger C, Mori T, Szekely CA, Tan J, Duman RS, Flavell RA. 2008. Blocking TGF-beta-Smad2/3 innate immune signaling mitigates Alzheimer-like pathology. *Nat Med* 14: 681-7

30. Naert G, Rivest S. 2012. Hematopoietic CC-chemokine receptor 2 (CCR2) competent cells are protective for the cognitive impairments and amyloid pathology in a transgenic mouse model of Alzheimer's disease. *Mol Med* 18: 297-313
31. Baruch K, Rosenzweig N, Kertser A, Deczkowska A, Sharif AM, Spinrad A, Tsitsou-Kampeli A, Sarel A, Cahalon L, Schwartz M. 2015. Breaking immune tolerance by targeting Foxp3(+) regulatory T cells mitigates Alzheimer's disease pathology. *Nat Commun* 6: 7967
32. Xing Z, Zuo Z, Hu D, Zheng X, Wang X, Yuan L, Zhou L, Qi F, Yao Z. 2020. Influenza vaccine combined with moderate-dose PD1 blockade reduces amyloid-beta accumulation and improves cognition in APP/PS1 mice. *Brain Behav Immun*
33. Baruch K, Deczkowska A, Rosenzweig N, Tsitsou-Kampeli A, Sharif AM, Matcovitch-Natan O, Kertser A, David E, Amit I, Schwartz M. 2016. PD-1 immune checkpoint blockade reduces pathology and improves memory in mouse models of Alzheimer's disease. *Nat Med* 22: 135-7
34. Zuroff L, Daley D, Black KL, Koronyo-Hamaoui M. 2017. Clearance of cerebral Abeta in Alzheimer's disease: reassessing the role of microglia and monocytes. *Cell Mol Life Sci* 74: 2167-201
35. Dionisio-Santos DA, Olschowka JA, O'Banion MK. 2019. Exploiting microglial and peripheral immune cell crosstalk to treat Alzheimer's disease. *J Neuroinflammation* 16: 74
36. Li Q, Barres BA. 2018. Microglia and macrophages in brain homeostasis and disease. *Nat Rev Immunol* 18: 225-42
37. Mosher KI, Wyss-Coray T. 2014. Microglial dysfunction in brain aging and Alzheimer's disease. *Biochem Pharmacol* 88: 594-604
38. Yu C, Roubeix C, Sennlaub F, Saban DR. 2020. Microglia versus Monocytes: Distinct Roles in Degenerative Diseases of the Retina. *Trends Neurosci* 43: 433-49
39. Wang Y, Cella M, Mallinson K, Ulrich JD, Young KL, Robinette ML, Gilfillan S, Krishnan GM, Sudhakar S, Zinselmeyer BH, Holtzman DM, Cirrito JR, Colonna M. 2015. TREM2 lipid sensing sustains the microglial response in an Alzheimer's disease model. *Cell* 160: 1061-71
40. Rosenzweig N, Dvir-Szternfeld R, Tsitsou-Kampeli A, Keren-Shaul H, Ben-Yehuda H, Weill-Raynal P, Cahalon L, Kertser A, Baruch K, Amit I, Weiner A, Schwartz M. 2019. PD-1/PD-L1 checkpoint blockade harnesses monocyte-derived macrophages to combat cognitive impairment in a tauopathy mouse model. *Nat Commun* 10: 465
41. Frenkel D, Wilkinson K, Zhao L, Hickman SE, Means TK, Puckett L, Farfara D, Kingery ND, Weiner HL, El Khoury J. 2013. Scara1 deficiency impairs clearance of soluble amyloid-beta by mononuclear phagocytes and accelerates Alzheimer's-like disease progression. *Nat Commun* 4: 2030
42. Jaitin DA, Kenigsberg E, Keren-Shaul H, Elefant N, Paul F, Zaretsky I, Mildner A, Cohen N, Jung S, Tanay A, Amit I. 2014. Massively parallel single-cell RNA-seq for marker-free decomposition of tissues into cell types. *Science* 343: 776-9
43. Keren-Shaul H, Kenigsberg E, Jaitin DA, David E, Paul F, Tanay A, Amit I. 2019. MARS-seq2.0: an experimental and analytical pipeline for indexed sorting combined with single-cell RNA sequencing. *Nat Protoc* 14: 1841-62

44. Baran Y, Bercovich A, Sebe-Pedros A, Lubling Y, Giladi A, Chomsky E, Meir Z, Hoichman M, Lifshitz A, Tanay A. 2019. MetaCell: analysis of single-cell RNA-seq data using K-nn graph partitions. *Genome Biol* 20: 206
45. Paul F, Arkin Y, Giladi A, Jaitin DA, Kenigsberg E, Keren-Shaul H, Winter D, Lara-Astiaso D, Gury M, Weiner A, David E, Cohen N, Lauridsen FK, Haas S, Schlitzer A, Mildner A, Ginhoux F, Jung S, Trumpp A, Porse BT, Tanay A, Amit I. 2015. Transcriptional Heterogeneity and Lineage Commitment in Myeloid Progenitors. *Cell* 163: 1663-77
46. Griciuc A, Patel S, Federico AN, Choi SH, Innes BJ, Oram MK, Cereghetti G, McGinty D, Anselmo A, Sadreyev RI, Hickman SE, El Khoury J, Colonna M, Tanzi RE. 2019. TREM2 Acts Downstream of CD33 in Modulating Microglial Pathology in Alzheimer's Disease. *Neuron* 103: 820-35 e7
47. Meilandt WJ, Ngu H, Gogineni A, Lalehzadeh G, Lee SH, Srinivasan K, Imperio J, Wu T, Weber M, Kruse AJ, Stark KL, Chan P, Kwong M, Modrusan Z, Friedman BA, Elstrott J, Foreman O, Easton A, Sheng M, Hansen DV. 2020. Trem2 Deletion Reduces Late-Stage Amyloid Plaque Accumulation, Elevates the Abeta42:Abeta40 Ratio, and Exacerbates Axonal Dystrophy and Dendritic Spine Loss in the PS2APP Alzheimer's Mouse Model. *J Neurosci* 40: 1956-74
48. Yuan P, Condello C, Keene CD, Wang Y, Bird TD, Paul SM, Luo W, Colonna M, Baddeley D, Grutzendler J. 2016. TREM2 Haplodeficiency in Mice and Humans Impairs the Microglia Barrier Function Leading to Decreased Amyloid Compaction and Severe Axonal Dystrophy. *Neuron* 90: 724-39
49. Benilova I, Karran E, De Strooper B. 2012. The toxic Abeta oligomer and Alzheimer's disease: an emperor in need of clothes. *Nat Neurosci* 15: 349-57
50. Yeh FL, Wang Y, Tom I, Gonzalez LC, Sheng M. 2016. TREM2 Binds to Apolipoproteins, Including APOE and CLU/APOJ, and Thereby Facilitates Uptake of Amyloid-Beta by Microglia. *Neuron* 91: 328-40
51. London A, Itskovich E, Benhar I, Kalchenko V, Mack M, Jung S, Schwartz M. 2011. Neuroprotection and progenitor cell renewal in the injured adult murine retina requires healing monocyte-derived macrophages. *J Exp Med* 208: 23-39
52. Vorhees CV, Williams MT. 2014. Assessing spatial learning and memory in rodents. *ILAR J* 55: 310-32
53. Wang Y, Ulland TK, Ulrich JD, Song W, Tzaferis JA, Hole JT, Yuan P, Mahan TE, Shi Y, Gilfillan S, Cella M, Grutzendler J, DeMattos RB, Cirrito JR, Holtzman DM, Colonna M. 2016. TREM2-mediated early microglial response limits diffusion and toxicity of amyloid plaques. *J Exp Med* 213: 667-75
54. Reed-Geaghan EG, Croxford AL, Becher B, Landreth GE. 2020. Plaque-associated myeloid cells derive from resident microglia in an Alzheimer's disease model. *J Exp Med* 217
55. Jordao MJC, Sankowski R, Brendecke SM, Sagar, Locatelli G, Tai YH, Tay TL, Schramm E, Armbruster S, Hagemeyer N, Gross O, Mai D, Cicek O, Falk T, Kerschensteiner M, Grun D, Prinz M. 2019. Single-cell profiling identifies myeloid cell subsets with distinct fates during neuroinflammation. *Science* 363: eaat7554
56. Shichita T, Ito M, Morita R, Komai K, Noguchi Y, Ooboshi H, Koshida R, Takahashi S, Kodama T, Yoshimura A. 2017. MAFB prevents excess inflammation after ischemic stroke by accelerating

clearance of damage signals through MSR1. *Nat Med* 23: 723-32

57. Amodio G, Cichy J, Conde P, Matteoli G, Moreau A, Ochando J, Oral BH, Pekarova M, Ryan EJ, Roth J, Sohrabi Y, Cuturi MC, Gregori S. 2019. Role of myeloid regulatory cells (MRCs) in maintaining tissue homeostasis and promoting tolerance in autoimmunity, inflammatory disease and transplantation. *Cancer Immunol Immunother* 68: 661-72
58. Bellavance MA, Gosselin D, Yong VW, Stys PK, Rivest S. 2015. Patrolling monocytes play a critical role in CX3CR1-mediated neuroprotection during excitotoxicity. *Brain Struct Funct* 220(3): 1759-76
59. Corps KN, Roth TL, McGavern DB. 2015. Inflammation and neuroprotection in traumatic brain injury. *JAMA Neurol* 72: 355-62
60. Fang W, Zhai X, Han D, Xiong X, Wang T, Zeng X, He S, Liu R, Miyata M, Xu B, Zhao H. 2018. CCR2-dependent monocytes/macrophages exacerbate acute brain injury but promote functional recovery after ischemic stroke in mice. *Theranostics* 8: 3530-43
61. Gliem M, Schwaninger M, Jander S. 2016. Protective features of peripheral monocytes/macrophages in stroke. *Biochim Biophys Acta* 1862: 329-38
62. Nahrendorf M, Pittet MJ, Swirski FK. 2010. Monocytes: protagonists of infarct inflammation and repair after myocardial infarction. *Circulation* 121: 2437-45
63. Latta-Mahieu M, Elmer B, Bretteville A, Wang Y, Lopez-Grancha M, Goniot P, Moindrot N, Ferrari P, Blanc V, Schussler N, Brault E, Roudieres V, Blanchard V, Yang ZY, Barneoud P, Bertrand P, Roucourt B, Carmans S, Bottelbergs A, Mertens L, Wintmolders C, Larsen P, Hersley C, McGathey T, Racke MM, Liu L, Lu J, O'Neill MJ, Riddell DR, Ebneth A, Nabel GJ, Pradier L. 2018. Systemic immune-checkpoint blockade with anti-PD1 antibodies does not alter cerebral amyloid-beta burden in several amyloid transgenic mouse models. *Glia* 66: 492-504
64. Goure WF, Krafft GA, Jerecic J, Hefti F. 2014. Targeting the proper amyloid-beta neuronal toxins: a path forward for Alzheimer's disease immunotherapeutics. *Alzheimers Res Ther* 6: 42
65. Cline EN, Bicca MA, Viola KL, Klein WL. 2018. The Amyloid-beta Oligomer Hypothesis: Beginning of the Third Decade. *J Alzheimers Dis* 64: S567-S610
66. Nelson PT, Alafuzoff I, Bigio EH, Bouras C, Braak H, Cairns NJ, Castellani RJ, Crain BJ, Davies P, Del Tredici K, Duyckaerts C, Frosch MP, Haroutunian V, Hof PR, Hulette CM, Hyman BT, Iwatsubo T, Jellinger KA, Jicha GA, Kovari E, Kukull WA, Leverenz JB, Love S, Mackenzie IR, Mann DM, Masliah E, McKee AC, Montine TJ, Morris JC, Schneider JA, Sonnen JA, Thal DR, Trojanowski JQ, Troncoso JC, Wisniewski T, Woltjer RL, Beach TG. 2012. Correlation of Alzheimer disease neuropathologic changes with cognitive status: a review of the literature. *J Neuropathol Exp Neurol* 71: 362-81
67. Tao Q, Ang TFA, DeCarli C, Auerbach SH, Devine S, Stein TD, Zhang X, Massaro J, Au R, Qiu WQ. 2018. Association of Chronic Low-grade Inflammation With Risk of Alzheimer Disease in ApoE4 Carriers. *JAMA Netw Open* 1: e183597
68. Misiak B, Leszek J, Kiejna A. 2012. Metabolic syndrome, mild cognitive impairment and Alzheimer's disease–the emerging role of systemic low-grade inflammation and adiposity. *Brain Res Bull* 89: 144-9

69. Ulland TK, Song WM, Huang SC, Ulrich JD, Sergushichev A, Beatty WL, Loboda AA, Zhou Y, Cairns NJ, Kambal A, Loginicheva E, Gilfillan S, Cella M, Virgin HW, Unanue ER, Wang Y, Artyomov MN, Holtzman DM, Colonna M. 2017. TREM2 Maintains Microglial Metabolic Fitness in Alzheimer's Disease. *Cell* 170: 649-63 e13

70. Alamed J, Wilcock DM, Diamond DM, Gordon MN, Morgan D. 2006. Two-day radial-arm water maze learning and memory task; robust resolution of amyloid-related memory deficits in transgenic mice. *Nat Protoc* 1: 1671-9

71. Bevins RA, Besheer J. 2006. Object recognition in rats and mice: a one-trial non-matching-to-sample learning task to study 'recognition memory'. *Nat Protoc* 1: 1306-11

Figures

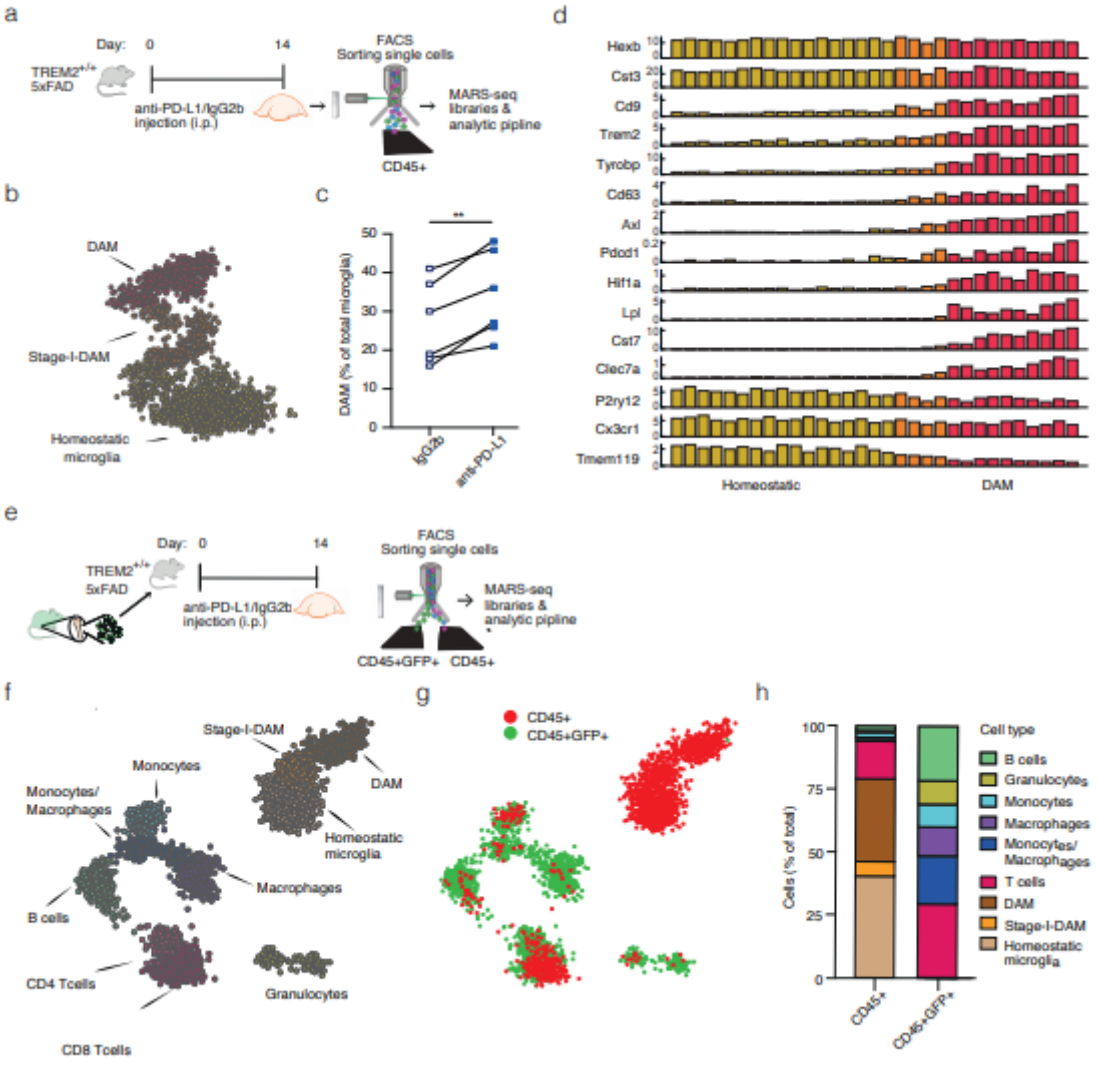

Figure 1

DAM cells are exclusively derived from resident microglia and their level is elevated following anti-PD-L1 treatment (a) Schematic presentation of the experimental design for testing the effect of anti-PD-L1 on microglia (b-d); CD45+ cells were collected for MARS-seq from brains of 6-7 month old Trem2+/+5xFAD mice, 14 days following injection of anti-PD-L1 or IgG2b. (b) 2D projection of 2931 microglia collected from anti-PD-L1 and IgG2b treated mice, arranged according to transcriptomic similarity, annotated and colored according to microglia/DAM signature of each metacell. (c) Percentage of DAM of total microglia in six pairs of littermate mice treated with anti-PD-L1/IgG2b. n=6 per group. ∗∗ $p<0.01$. (d) Multiple bar graphs showing the expression level (average UMI/cell) of selected marker genes across 31 microglia metacells isolated from the brains of both anti-PD-L1 and IgG2b treated mice. Metacells are arranged from left to right based on activation level, and colored accordingly (red - DAM, orange - stage-I-DAM, yellow - resting microglia). (e) Schematic presentation of the experimental design for testing the origin of DAM (f-h); 8-month old BM-chimeric mice (Trem2+/+5xFAD transplanted with Ub-GFP WT BM) were injected with either anti-PD-L1 or IgG2b, and 14 days later CD45+ and CD45+GFP+ cells were collected for MARS-seq. (f, g) 2D projection of 3531 cells from both CD45+ and CD45+GFP+ plates, clustered according to transcriptomic similarity; color coding represents cell type annotation (f), and the source of each cell - either CD45+ or CD45+GFP+ (g). (h) Bar graph showing the relative contribution of each cell type to the pool of CD45+ and CD45+GFP+ sorted cells (anti-PD-L1 and IgG2b treated AD mice are pooled together).

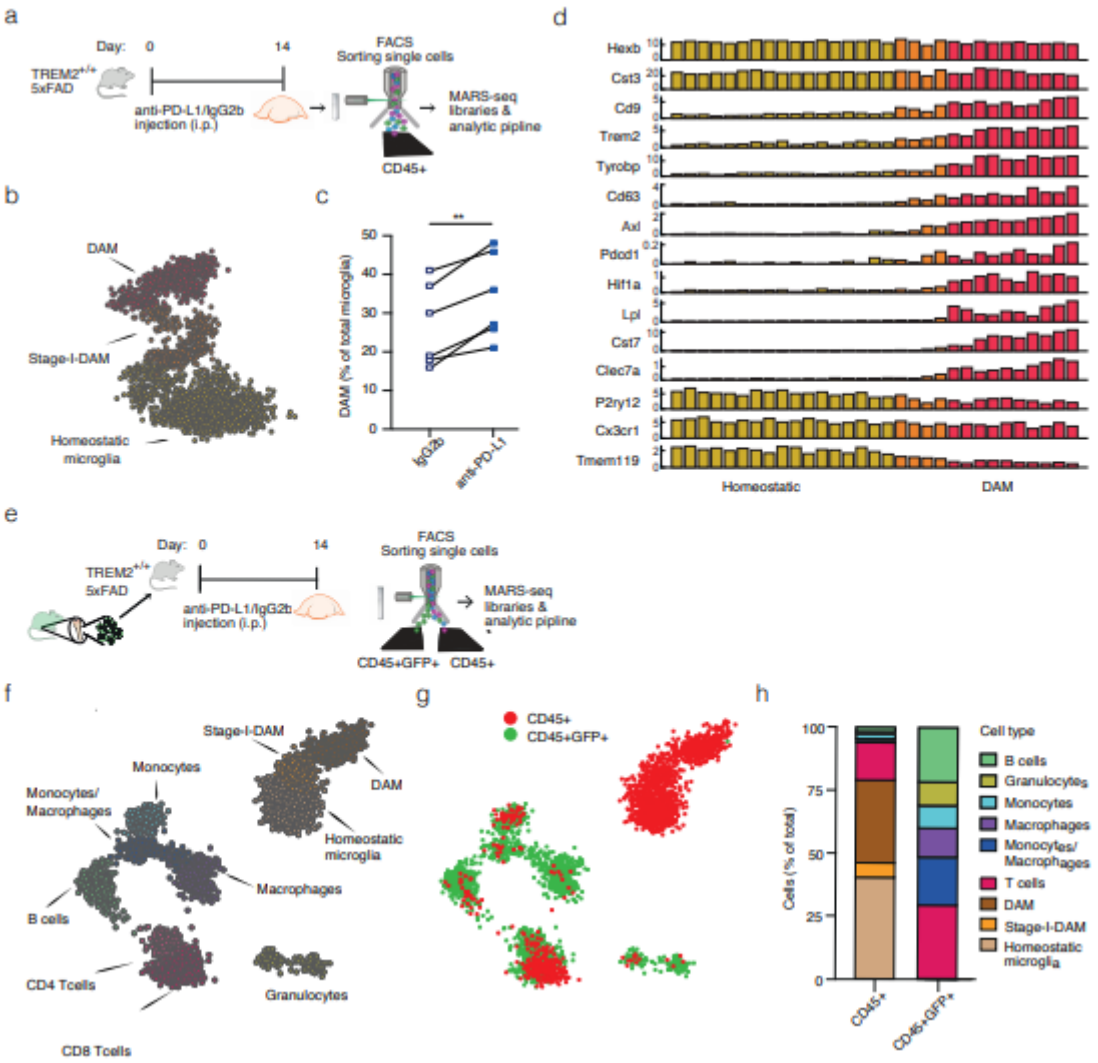

Figure 1

DAM cells are exclusively derived from resident microglia and their level is elevated following anti-PD-L1 treatment (a) Schematic presentation of the experimental design for testing the effect of anti-PD-L1 on microglia (b-d); CD45+ cells were collected for MARS-seq from brains of 6-7 month old Trem2+/+5xFAD mice, 14 days following injection of anti-PD-L1 or IgG2b. (b) 2D projection of 2931 microglia collected from anti-PD-L1 and IgG2b treated mice, arranged according to transcriptomic similarity, annotated and colored according to microglia/DAM signature of each metacell. (c) Percentage of DAM of total microglia in six pairs of littermate mice treated with anti-PD-L1/IgG2b. n=6 per group. ∗∗ p<0.01. (d) Multiple bar graphs showing the expression level (average UMI/cell) of selected marker genes across 31 microglia metacells isolated from the brains of both anti-PD-L1 and IgG2b treated mice. Metacells are arranged from left to right based on activation level, and colored accordingly (red - DAM, orange - stage-I-DAM, yellow - resting microglia). (e) Schematic presentation of the experimental design for testing the origin of DAM (f-h); 8-month old BM-chimeric mice (Trem2+/+5xFAD transplanted with Ub-GFP WT BM) were injected with either anti-PD-L1 or IgG2b, and 14 days later CD45+ and CD45+GFP+ cells were collected for MARS-seq. (f, g) 2D projection of 3531 cells from both CD45+ and CD45+GFP+ plates, clustered

according to transcriptomic similarity; color coding represents cell type annotation (f), and the source of each cell - either CD45+ or CD45+GFP+ (g). (h) Bar graph showing the relative contribution of each cell type to the pool of CD45+ and CD45+GFP+ sorted cells (anti-PD-L1 and IgG2b treated AD mice are pooled together).

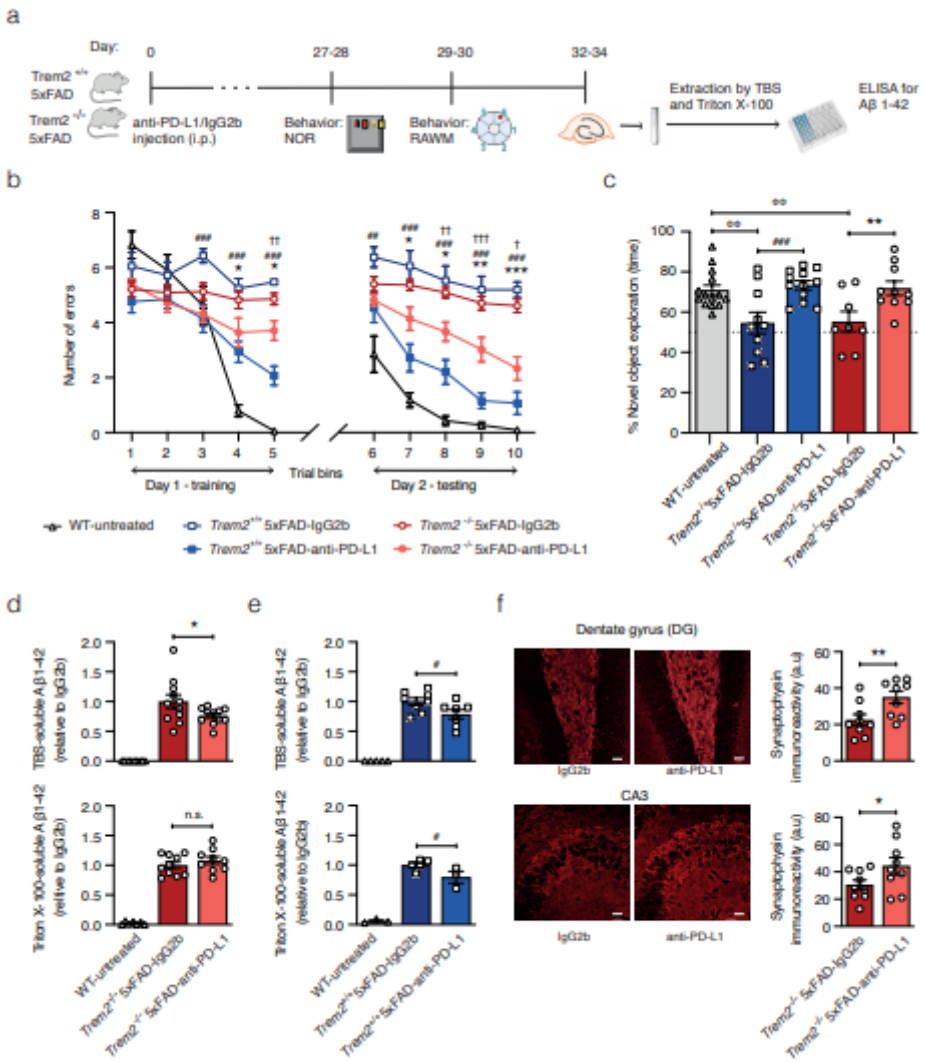

Figure 2

Treatment with anti-PD-L1 antibody ameliorates AD pathology and induces neuroprotection in Trem2-deficient mice (a) Schematic presentation of the experimental design for testing the effect of anti-PD-L1 on AD pathology in Trem2+/+5xFAD and Trem2-/-5xFAD mice; 6-9 month old Trem2+/+5xFAD and Trem2-/-5xFAD mice were treated i.p. with either anti-PD-L1 or IgG2b control antibody. After 27-30 days, cognitive performance was assessed by RAWM and NOR tasks and, 2 days later, hippocampi from one hemisphere were processed for Aβ1-42 ELISA; age matched WT mice, both Trem2+/+ and Trem2-/-, were included as controls. (b) RAWM performance of Trem2+/+5xFAD and Trem2-/-5xFAD mice, treated with anti-PD-L1 or IgG2b, and of WT controls, presented as the number of errors made, averaged per every 3 trials, on the x axis. (two-way ANOVA and Fisher's LSD test) (d) NOR performance of all groups presented as the percentage of novel object exploration of total exploration time (One-way ANOVA and Fisher's LSD

test). WT (both Trem2+/+ and Trem2-/-) n=14, Trem2+/+5xFAD/IgG2b n=10, Trem2+/+5xFAD/anti-PD-L1 n=12, Trem2-/-5xFAD/IgG2b n=8, Trem2-/-5xFAD/anti-PD-L1 n=10; b,c. (d) ELISA assessment of Aβ1-42 TBS-soluble and Triton-X-100-soluble hippocampal fractions from anti-PD-L1 and IgG2b treated Trem2-/-5xFAD and untreated Trem2-/-WT; n=9-11 per group (e) ELISA assessment of Aβ1-42 TBS-soluble and Triton-X-100-soluble hippocampal fractions from anti-PD-L1 and IgG2b treated Trem2+/+5xFAD and untreated Trem2+/+WT; n=3-8 per group. (one-way ANOVA and Fisher's LSD test, d,e). (f) Representative immunofluorescence images and quantitative analysis of synaptophysin-immunoreactivity in the DG and the hippocampal CA3 regions, in the brains of anti-PD-L1 and IgG2b treated Trem2-/-5xFAD mice. n=9 per group; (one-tailed Student's t test). Scale bars, 50 μm. Data in all graphs are shown as mean ± SEM; * relates to the comparison between anti-PD-L1 and IgG2 treated Trem2-/-5xFAD mice; # relates to the comparison between anti-PD-L1 and IgG2 treated Trem2+/+5xFAD mice; † relates to the comparison between anti-PD-L1 treated Trem2-/-5xFAD and Trem2+/+5xFAD mice Φ relates to the comparison with WT.*,#,†, Φ p<0.05, ##,**,††, Φ Φ p<0.01, ###,***,†††, Φ Φ Φ p<0.001.

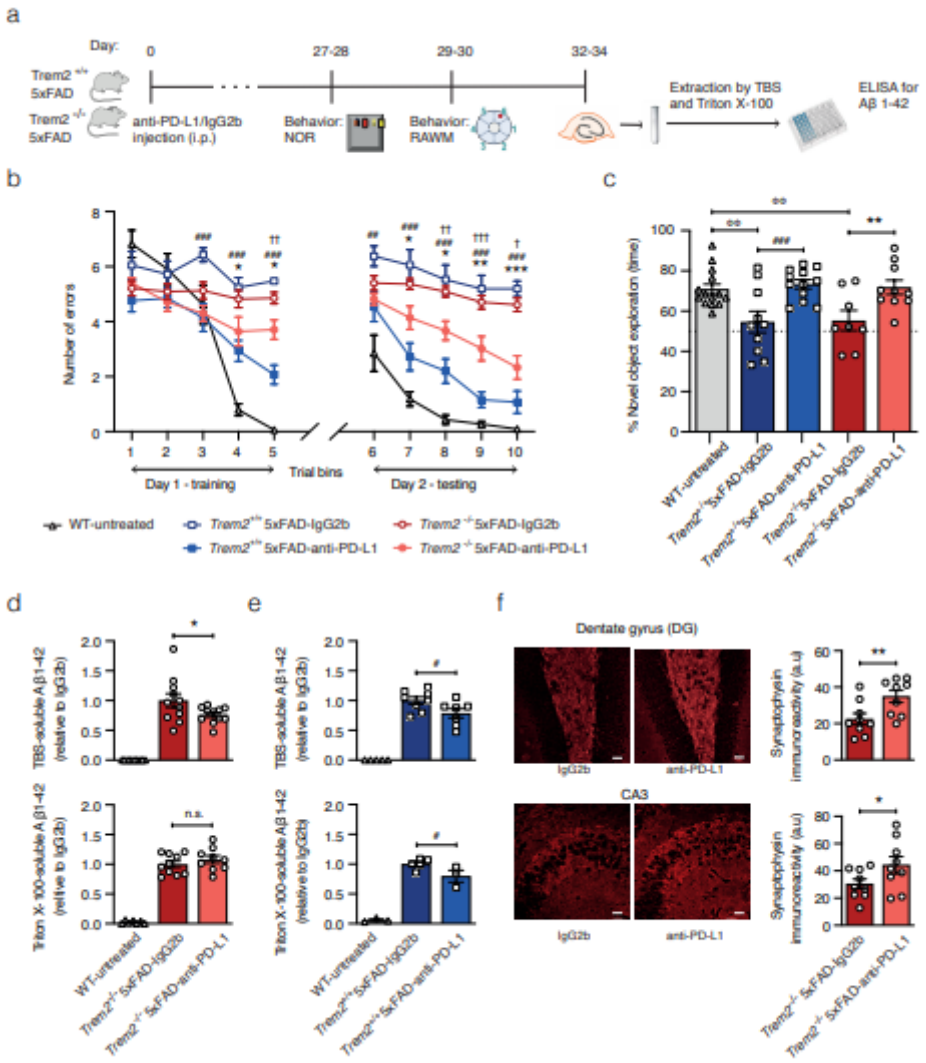

Figure 2

Treatment with anti-PD-L1 antibody ameliorates AD pathology and induces neuroprotection in Trem2-deficient mice (a) Schematic presentation of the experimental design for testing the effect of anti-PD-L1 on AD pathology in Trem2+/+5xFAD and Trem2-/-5xFAD mice; 6-9 month old Trem2+/+5xFAD and Trem2-/-5xFAD mice were treated i.p. with either anti-PD-L1 or IgG2b control antibody. After 27-30 days, cognitive performance was assessed by RAWM and NOR tasks and, 2 days later, hippocampi from one hemisphere were processed for Aβ1-42 ELISA; age matched WT mice, both Trem2+/+ and Trem2-/-, were included as controls. (b) RAWM performance of Trem2+/+5xFAD and Trem2-/-5xFAD mice, treated with anti-PD-L1 or IgG2b, and of WT controls, presented as the number of errors made, averaged per every 3 trials, on the x axis. (two-way ANOVA and Fisher's LSD test) (d) NOR performance of all groups presented as the percentage of novel object exploration of total exploration time (One-way ANOVA and Fisher's LSD test). WT (both Trem2+/+ and Trem2-/-) n=14, Trem2+/+5xFAD/IgG2b n=10, Trem2+/+5xFAD/anti-PD-L1 n=12, Trem2-/-5xFAD/IgG2b n=8, Trem2-/-5xFAD/anti-PD-L1 n=10; b,c. (d) ELISA assessment of Aβ1-42 TBS-soluble and Triton-X-100-soluble hippocampal fractions from anti-PD-L1 and IgG2b treated Trem2-/-5xFAD and untreated Trem2-/-WT; n=9-11 per group (e) ELISA assessment of Aβ1-42 TBS-soluble and Triton-X-100-soluble hippocampal fractions from anti-PD-L1 and IgG2b treated Trem2+/+5xFAD and untreated Trem2+/+WT; n=3-8 per group. (one-way ANOVA and Fisher's LSD test, d,e). (f) Representative immunofluorescence images and quantitative analysis of synaptophysin-immunoreactivity in the DG and the hippocampal CA3 regions, in the brains of anti-PD-L1 and IgG2b treated Trem2-/-5xFAD mice. n=9 per group; (one-tailed Student's t test). Scale bars, 50 μm. Data in all graphs are shown as mean ± SEM; * relates to the comparison between anti-PD-L1 and IgG2 treated Trem2-/-5xFAD mice; # relates to the comparison between anti-PD-L1 and IgG2 treated Trem2+/+5xFAD mice; † relates to the comparison between anti-PD-L1 treated Trem2-/-5xFAD and Trem2+/+5xFAD mice Φ relates to the comparison with WT.*,#,†, Φ $p<0.05$, ##,**,††, Φ Φ $p<0.01$, ###,***,†††, Φ Φ Φ $p<0.001$.

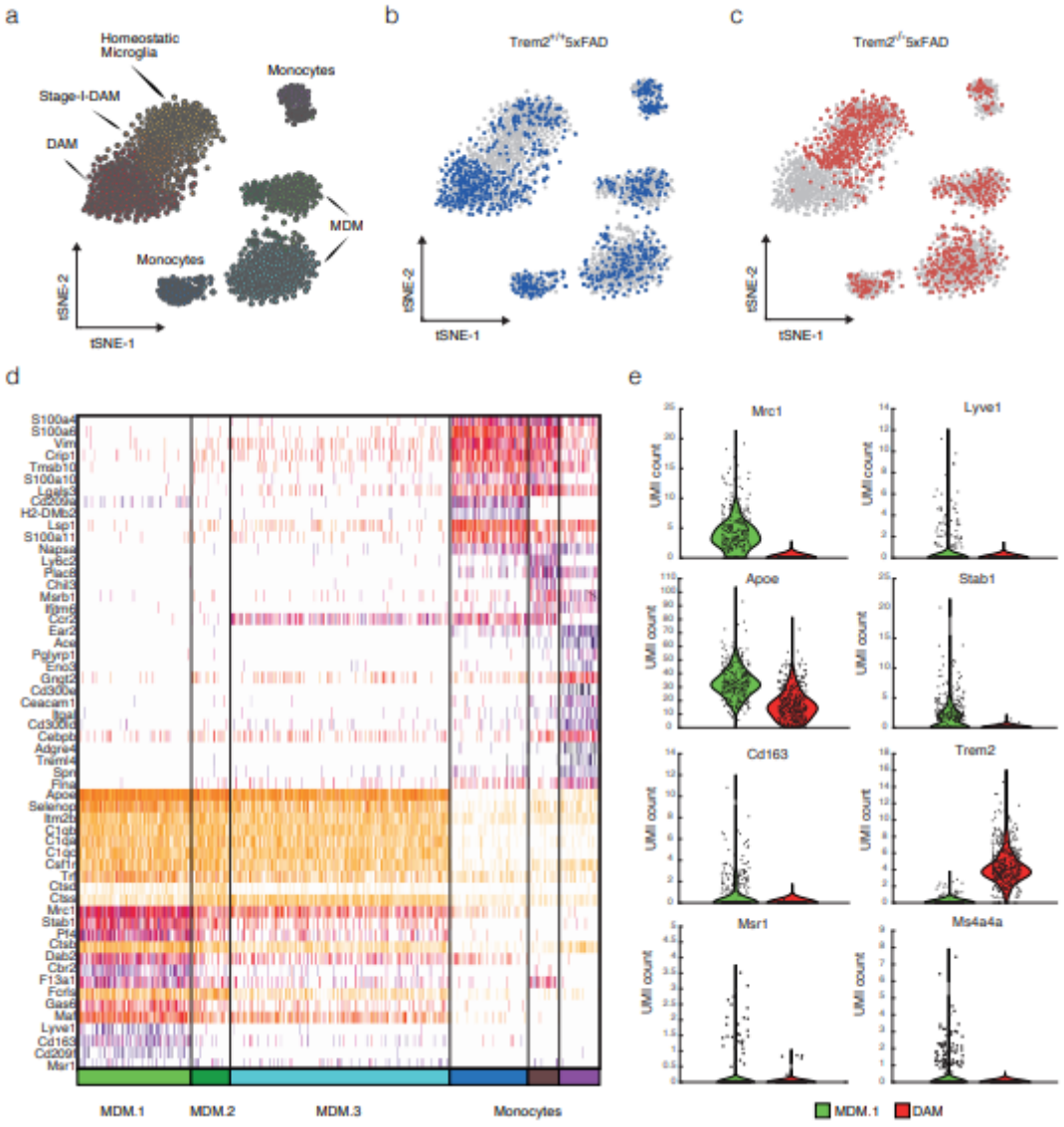

Figure 3

Monocyte-derived macrophages express a unique transcriptomic signature in both Trem2+/+5xFAD and Trem2-/-5xFAD brains (a-c) tSNE plot of 2290 myeloid cells (CD45highCD11bhigh) isolated from Trem2+/+5xFAD and Trem2-/-5xFAD brains, 14 days following injection of anti-PD-L1 or IgG2b, colored for cluster annotation (a), and highlighted according to source mouse strain, Trem2+/+5xFAD (b) and Trem2-/-5xFAD (c). (d) Heatmap showing clustering analysis of 1181 non-microglia myeloid cells, featuring the most variable genes. Color coding at the bottom bar corresponds to a. (e) Violin plots comparing UMI count of selected genes between MDM-1 and DAM.

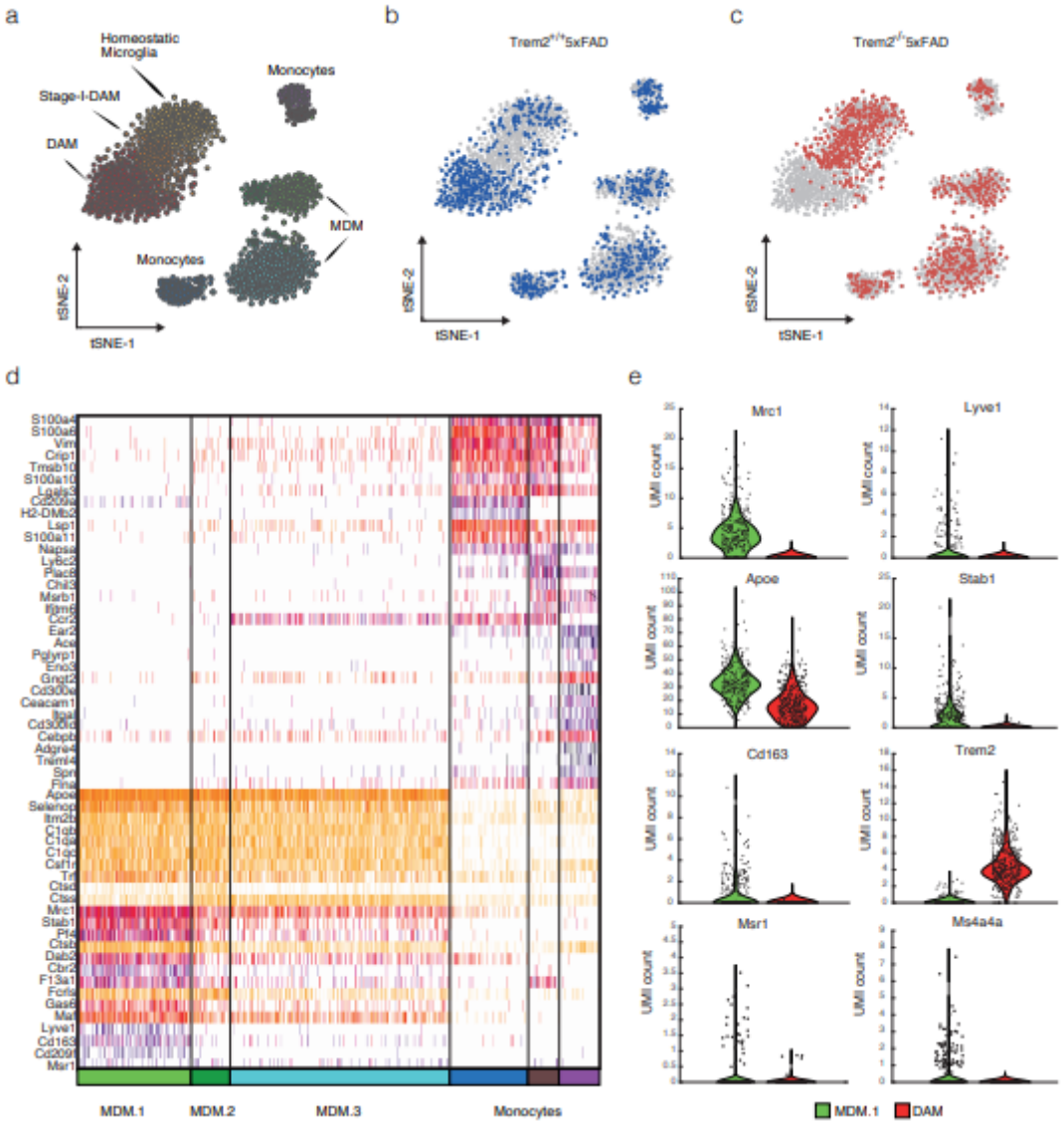

Figure 3

Monocyte-derived macrophages express a unique transcriptomic signature in both Trem2+/+5xFAD and Trem2-/-5xFAD brains (a-c) tSNE plot of 2290 myeloid cells (CD45highCD11bhigh) isolated from Trem2+/+5xFAD and Trem2-/-5xFAD brains, 14 days following injection of anti-PD-L1 or IgG2b, colored for cluster annotation (a), and highlighted according to source mouse strain, Trem2+/+5xFAD (b) and Trem2-/-5xFAD (c). (d) Heatmap showing clustering analysis of 1181 non-microglia myeloid cells, featuring the most variable genes. Color coding at the bottom bar corresponds to a. (e) Violin plots comparing UMI count of selected genes between MDM-1 and DAM.

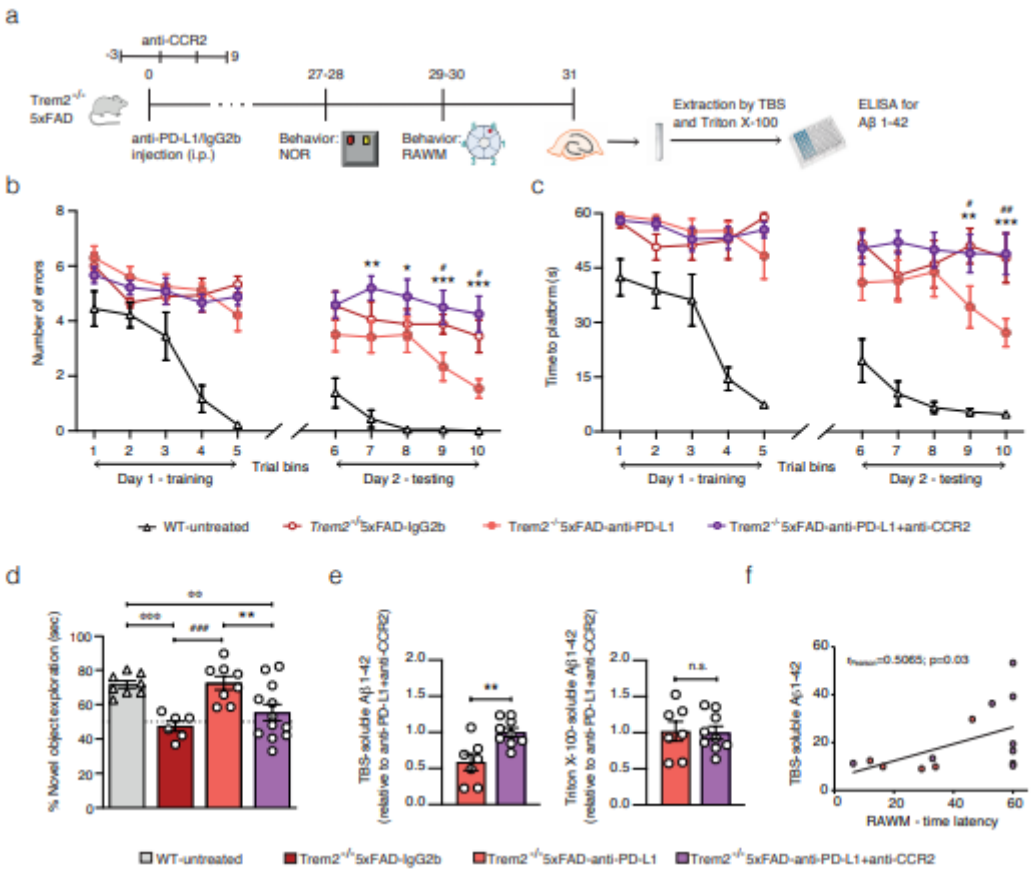

Figure 4

Eliminating monocytes using CCR2 blocking antibody abrogates the beneficial effects of anti-PD-L1 treatment on cognition and on soluble Aβ1-42 removal (a) Schematic presentation of the experimental design for testing the impact of monocyte elimination on the effect of anti-PD-L1 treatment in Trem2-/-5xFAD mice; 7-8 month old Trem2-/-5xFAD mice were treated i.p. with anti-PD-L1 antibody, with or without four doses of anti-CCR2 antibody administered i.p; another group received only the IgG2b control antibody. After 27-30 days, cognitive performance was assessed by RAWM and NOR tasks and, a day later, hippocampi from both hemispheres were processed for ELISA of Aβ1-42; age matched WT Trem2-/- mice were included as controls. (b,c) RAWM performance of Trem2-/-5xFAD mice, treated with anti-PD-L1 and with anti-CCR2 (anti-PD-L1+anti-CCR2), anti-PD-L1 and IgG2b, and of WT controls, presented as the number of errors made (b) and as the latency to platform (c), averaged per every three trials, on the x axis (two-way ANOVA and Fisher's LSD test). (d) NOR performance of all groups presented as the percentage of novel object exploration of total exploration time (One-way ANOVA and Fisher's LSD test); Trem2-/-WT n=8, Trem2-/-5xFAD/IgG2b n=6, Trem2-/-5xFAD/anti-PD-L1 n=8, Trem2-/-5xFAD/anti-PD-L1+anti-CCR2 n=12. (e) ELISA assessment of Aβ1-42 TBS-soluble and Triton-X-100-soluble hippocampal fractions from anti-PD-L1 and anti-PD-L1+anti-CCR2 treated Trem2-/-5xFAD mice. Due to technical limitations, samples representing both experimental groups were run in two batches. The values shown on the Y-axes represent the ratio between the level of each sample and the average of anti-PD-L1+anti-CCR2 in the same batch (one-tailed Student's t test); n=7-9 per group. (f) Correlation between the

values of TBS-soluble Aβ1-42 ELISA, corresponding to (e, left panel), and RAWM time latency, corresponding to (c) of the same mice. Data in all graphs are shown as mean ± SEM; * relates to the comparison between anti-PD-L1 and anti-PD-L1+anti-CCR2; # relates to the comparison between anti-PD-L1 and IgG; Φ relates to the comparison with WT. *,#, Φ p<0.05, ##,**, Φ Φ p<0.01, ###,***, Φ Φ Φ p<0.001.

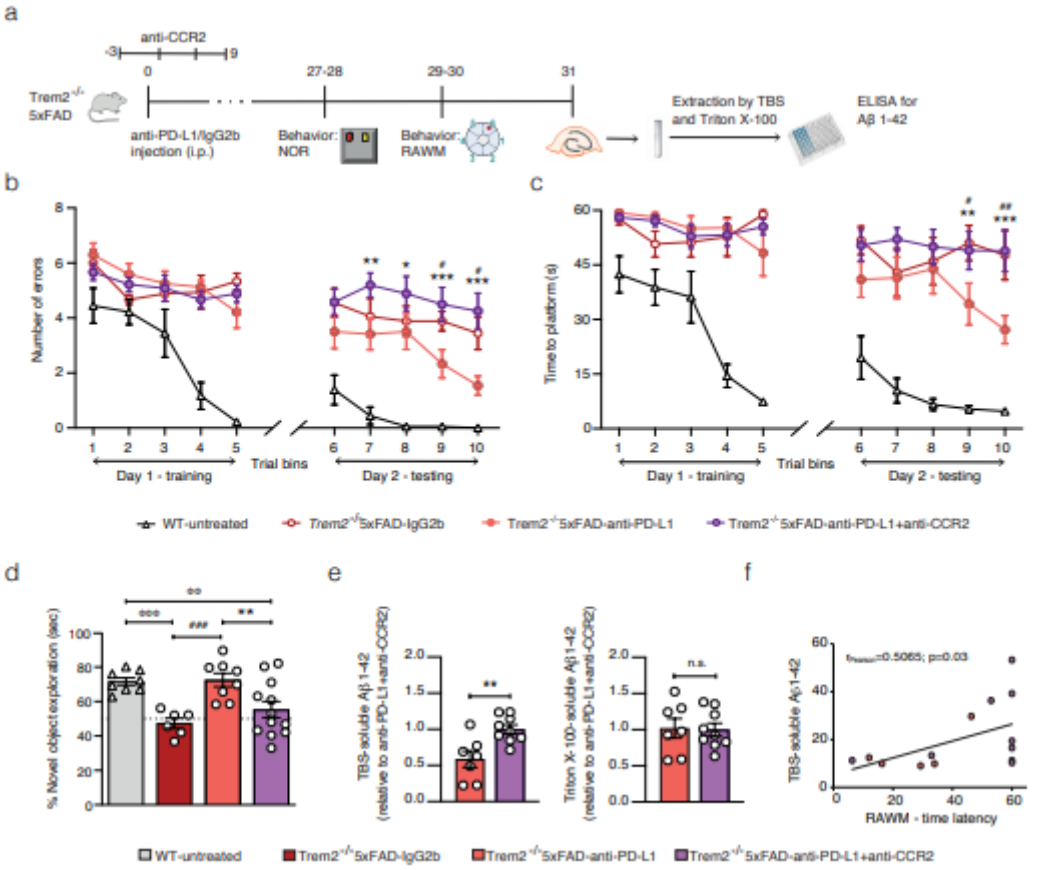

Figure 4

Eliminating monocytes using CCR2 blocking antibody abrogates the beneficial effects of anti-PD-L1 treatment on cognition and on soluble Aβ1-42 removal (a) Schematic presentation of the experimental design for testing the impact of monocyte elimination on the effect of anti-PD-L1 treatment in Trem2-/-5xFAD mice; 7-8 month old Trem2-/-5xFAD mice were treated i.p. with anti-PD-L1 antibody, with or without four doses of anti-CCR2 antibody administered i.p; another group received only the IgG2b control antibody. After 27-30 days, cognitive performance was assessed by RAWM and NOR tasks and, a day later, hippocampi from both hemispheres were processed for ELISA of Aβ1-42; age matched WT Trem2-/- mice were included as controls. (b,c) RAWM performance of Trem2-/-5xFAD mice, treated with anti-PD-L1 and with anti-CCR2 (anti-PD-L1+anti-CCR2), anti-PD-L1 and IgG2b, and of WT controls, presented as the number of errors made (b) and as the latency to platform (c), averaged per every three trials, on the x axis (two-way ANOVA and Fisher's LSD test). (d) NOR performance of all groups presented as the percentage of novel object exploration of total exploration time (One-way ANOVA and Fisher's LSD test); Trem2-/-WT n=8, Trem2-/-5xFAD/IgG2b n=6, Trem2-/-5xFAD/anti-PD-L1 n=8, Trem2-/-5xFAD/anti-PD-L1+anti-CCR2 n=12. (e) ELISA assessment of Aβ1-42 TBS-soluble and Triton-X-100-soluble

hippocampal fractions from anti-PD-L1 and anti-PD-L1+anti-CCR2 treated Trem2-/-5xFAD mice. Due to technical limitations, samples representing both experimental groups were run in two batches. The values shown on the Y-axes represent the ratio between the level of each sample and the average of anti-PD-L1+anti-CCR2 in the same batch (one-tailed Student's t test); n=7-9 per group. (f) Correlation between the values of TBS-soluble Aβ1-42 ELISA, corresponding to (e, left panel), and RAWM time latency, corresponding to (c) of the same mice. Data in all graphs are shown as mean ± SEM; * relates to the comparison between anti-PD-L1 and anti-PD-L1+anti-CCR2; # relates to the comparison between anti-PD-L1 and IgG; Φ relates to the comparison with WT. *,#, Φ p<0.05, ##,**, Φ Φ p<0.01, ###,***, Φ Φ Φ p<0.001.

Supplementary Files

This is a list of supplementary files associated with this preprint. Click to download.

- SuppFig1.pdf
- SuppFig1.pdf
- SuppFig2.pdf
- SuppFig2.pdf
- SuppFig3.pdf
- SuppFig3.pdf
- SuppFig4.pdf
- SuppFig4.pdf
- StatisticssummaryNA.pdf
- StatisticssummaryNA.pdf